

Dalton Transactions

Accepted Manuscript



This is an *Accepted Manuscript*, which has been through the Royal Society of Chemistry peer review process and has been accepted for publication.

Accepted Manuscripts are published online shortly after acceptance, before technical editing, formatting and proof reading. Using this free service, authors can make their results available to the community, in citable form, before we publish the edited article. We will replace this *Accepted Manuscript* with the edited and formatted *Advance Article* as soon as it is available.

You can find more information about *Accepted Manuscripts* in the [Information for Authors](#).

Please note that technical editing may introduce minor changes to the text and/or graphics, which may alter content. The journal's standard [Terms & Conditions](#) and the [Ethical guidelines](#) still apply. In no event shall the Royal Society of Chemistry be held responsible for any errors or omissions in this *Accepted Manuscript* or any consequences arising from the use of any information it contains.

**Concentration quenching of praseodymium ions Pr³⁺ in
BaGd₂(MoO₄)₄ crystals**

Ying Guan,^a Taiju Tsuboi,^{b,c} Yanlin Huang^{*a} and Wei Huang^{*b}

a College of Chemistry, Chemical Engineering and Materials Science, Soochow University,

Suzhou 215123, China

b Institute of Advanced Materials, Nanjing University of Technology, 5 XinMoFan Road, Nanjing

210009, China

c Faculty of Engineering, Kyoto Sangyo University, Kyoto 603-8555, Japan

*Author to whom correspondence should be address: wei-huang@njut.edu.cn (Wei Huang), Tel.: +86-25-58139001, Fax: +86-25-58139988. huang@suda.edu.cn (Y. Huang), Tel.: +86-13584875529, Fax: +86-512-65880089.

Abstract:

Concentration effect on the photoluminescence (PL) of praseodymium Pr^{3+} ion is studied at 298-12 K for barium gadolinium molybdate ($\text{BaGd}_2(\text{MoO}_4)_4$, called BGM) crystals with a wide Pr^{3+} concentration range of 0.05-25.0 mol %. Three types of concentration dependences are observed for the emissions although all types show the PL quenching at high concentrations. The first type (Type A) has the maximum PL intensity at about 10 mol % with non-zero intensity at high concentrations, which is observed for the $^3\text{P}_0$ emissions except emission at 621 nm. The second and third types (Type B-1 and B-2) have the maximum at about 1 mol % with a finite residual intensity and nearly zero intensity at high concentrations, respectively, which are observed for the 621 nm emission and all the $^1\text{D}_2$ emissions. It is suggested that the energy migration mechanism is responsible for Type A, while the non-resonant cross-relaxation for Type B-1 and the resonant cross-relaxation for Type B-2.

Keywords: Pr^{3+} ion; Rare earth spectroscopy; Photoluminescence; Concentration quenching; Cross-relaxation; Energy migration; Molybdate

1. Introduction

It is well-known that the photoluminescence (PL) of rare-earth ions like trivalent praseodymium ion (Pr^{3+}) doped in inorganic materials is quenched as the rare-earth concentration increased. Two main processes have been suggested as the reasons for this concentration quenching.¹⁻¹⁰ One is cross-relaxation (CR) process, the other is the energy migration. The former process occurs between two neighbouring rare-earth ions, while the latter process occurs over rare-earth ions in crystal and the migration stops at the quenching sites.

The CR process is described as follows. When one ion A in an excited state with energy E_{A1} is relaxed into a lower excited state with energy E_{A2} , a part of its energy $E_{A1}-E_{A2}$ is transferred to the neighboring ion B in the ground state with energy E_{B1} , leading to excitation into the excited state with energy E_{B2} if $E_{B2}-E_{B1}$ is almost the same as $E_{A1}-E_{A2}$. In case that $E_{B2}-E_{B1}$ is exactly the same with $E_{A1}-E_{A2}$, it is called resonant CR process, while in the case that $E_{B2}-E_{B1}$ is nearly same as $E_{A1}-E_{A2}$, it is called non-resonant CR process.

The CR is an essential factor to determine the quality and efficiency of rare-earth solid state lasers, optical amplifiers, scintillation detectors, phosphors, and sensors. The CR of Pr^{3+} ions has been reported for various host materials, e.g., YPO_4 , LaAlO_3 , $\text{Gd}_3\text{Ga}_5\text{O}_{12}$, and $\text{Y}_4\text{Al}_2\text{O}_9$.^{1-4,10-13} Regarding $\text{BaGd}_2(\text{MoO}_4)_4$ (called BGM hereafter) doped with Pr^{3+} ions, no work has been made although BGM host material shows an efficient laser action.¹⁴⁻¹⁶

Most investigations on the concentration quenching of Pr^{3+} -doped crystals have

been made in a limited concentration range such as 0.1-2 % or 0.005-0.1 % and at a limited temperature of room temperature. Therefore a clear answer has not been established to the questions that “Which concentration does Pr^{3+} -doped crystal give the maximum emission intensity?” and “Do all the Pr^{3+} emissions show the same concentration dependence?”. If these would be clarified, we can choose the best doping concentration of Pr^{3+} ions to reduce the effect of concentration quenching and obtain high emission intensity.

In the present paper, we investigate the PL spectra of Pr^{3+} ions doped BGM in a very wide concentration range from very low (0.05 mol %) to very high (25 mol %) at not only room temperature but also 12 K, to obtain more precise concentration dependence and to clarify its mechanism. One of the new findings is that resonant CR gives rise to different concentration dependences from non-resonant CR.

2. Experimental

Polycrystalline samples of $\text{BaGd}_{2-x}\text{Pr}_x(\text{MoO}_4)_4$ with various Pr^{3+} concentrations x were synthesized via the solid-state reaction, where $x = 0.001, 0.01, 0.02, 0.06, 0.1, 0.14, 0.2, 0.3, 0.4,$ and 0.5 (i.e., Pr^{3+} concentrations of 0.05, 0.5, 1.0, 3.0, 5.0, 7.0, 10, 15, 20, and 25 mol %), which are called Pr1, Pr2, Pr3, Pr4, Pr5, Pr6, Pr7, Pr8, Pr9, and Pr10, respectively. The starting material was a stoichiometric mixture of BaCO_3 , Gd_2O_3 , Pr_6O_{11} , and $(\text{NH}_4)_6\text{MO}_7\text{O}_{24}\cdot 4\text{H}_2\text{O}$. Firstly, the stoichiometric mixture was slowly heated up to 350 °C in 5 h and kept at this temperature for 5 h. The obtained powder was mixed again and then heated up to 780 °C for 5 h in air. After that, the

sample was thoroughly mixed and heated at 880 °C for 10 h in air.

The X-ray diffraction (XRD) pattern was collected on a Rigaku D/Max diffractometer operating at 40 kV, 30 mA with Bragg–Brentano geometry using Cu K α radiation ($\lambda=0.15405$ nm) and analyzed by using Jade-5.0 software Program.

PL excitation (PLE) and PL spectra were measured with a Horiba-Spex Fluorolog-3 spectrophotometer under a 500 W Xe-lamp excitation at various temperatures from 298 K to 12 K. Infrared luminescence spectra were measured in a spectral range between 800 and 1600 nm using a liquid-nitrogen cooled Jobin-Yvon DSS-IGA020L InGaAs photo-diode, while visible luminescence spectra were measured with a Hamamatsu-Photonics R928P photomultiplier. The samples were cooled down from room temperature (298 K) to temperatures around 12 K using an Iwatani Industrial Gas Corp. Cryo-Mini cryogenic refrigerator, which has a compressor containing He-gas, i.e., a closed cycle helium cryostat.

Raman spectra were measured with a Lambda Vision RAM-532 Raman spectrometer at room temperature using a 532 nm laser with a power of 70 mW. Luminescence decays were obtained at room temperature using a Horiba fluorescence decay profile equipment FluoroCube System 5000S which is operated by the time correlated single photon counting (TCSPC) method. The excitation was made by a Xe flash lamp.

3. Results and discussions

3.1 X-ray diffraction patterns and Raman spectra

Identical XRD patterns were obtained for the samples PrN (N=1, 3, 5, 6, 8, and 10) with different Pr³⁺ concentrations from 0.05 mol % to 25 mol % (Fig. 1), which are quite similar to the previously obtained XRD patterns of BGM crystals,¹⁷ and agree with JCPDS card 36-0192 of BaGd₂(MoO₄)₄.¹⁸ All peaks except the weak peak at 22.6° (indicated by (*)) are in good agreement with the PDF#2 No: 36-0192 although this standard card gives the XRD peaks in limited angles of 14-50° and it shows a small peak shift for all the XRD peaks. The 22.6° peak seems to arise from impurities.

From the XRD patterns, it is suggested that the doping of Pr³⁺ ions does not give influence on the host structure. No peak corresponding to praseodymium compound is observed, demonstrating that Pr³⁺ ions are uniformly dispersed in the host matrix even in heavily doped crystals. From this result, we confirm that our samples are successfully synthesized and the obtained BGM crystals keep the structure of space group *C2/c* with a MoO₄ tetrahedron and a GdO₈ polyhedron.¹⁹

The Raman spectra were measured for four PrN (N=1, 6, 9, and 10) samples to estimate the phonon energy of BGM. All the Raman spectra are quite similar to each other, with two intense peaks at 944 and 852 cm⁻¹ and a weak peak at 410 cm⁻¹ (Fig. 2). It is suggested from the observed Raman spectra that (1) the phonon modes of Pr³⁺-doped BGM crystal do not depend on the Pr³⁺ concentration and (2) the Pr-Pr interaction in highly doped crystals does not give any effect on the phonon modes.

3.2 Level assignment of emission lines

The PL spectra of Pr2 at 290 and 12 K are shown in **Fig. 3**. Sharp lines are observed at about 490, 500, 558, 602, 606, 608, 615, 621, 623, 651, 690, 716, 736, 824, and 830 nm at 12 K. These emissions are observed for all the samples of Pr1-Pr10, although the emissions at 602, 606, 608, and 615 nm are too weak to observe in Pr7-Pr10 with high concentrations.

The assignment for the observed emissions has been made using the energy level diagram of $(4f)^2$ electron configuration in Pr^{3+} ion, which is given by Dieke and Crosswhite.^{11,20-23} The level assignments for all the observed emissions are shown in **Fig. 4**. The reasonability of these assignments is checked from the PLE spectra. For example, the emission at 690 nm has PLE peaks at 602 and 593 nm, while another emission at 736 nm has no PLE peaks at 602 and 593 nm (**Fig. 5**). This indicates that the 736 nm emission certainly arises from the $^3\text{P}_0$ state, while the 690 nm emission arises from the $^1\text{D}_2$ state. Sharp peaks are observed at 488, 475, 464, 458, and 450 nm in the PLE spectra from the two emission spectra. Therefore it is confirmed that the weak 690 and 736 nm emissions are not due to unwanted impurities but due to Pr^{3+} ions.

3.3 Concentration dependence of PL spectra

3.3.1 Three types of concentration dependence

Figure 6 shows the PL spectra at various Pr^{3+} concentrations between 0.05 and 25 mol % at room temperature. When the concentration is increased from 0.05 mol %, the intensity of the 651 nm emission increases until the concentration becomes about 10 mol %, and decreases gradually above 10 mol % (**Fig. 7**). The 651 nm emission,

however, never disappears even at high concentrations. Same behavior was obtained for the 490, 558, and 736 nm emissions. The intensity ratios among the 490, 558, 651, and 736 nm emissions do not change with the variation of concentrations, indicating these emissions arise from the same 3P_0 state (Fig. 4).

The 602 nm emission shows quite different concentration dependence from the 490, 558, 651, and 736 nm emissions. Its emission intensity increases rapidly with increasing concentration from 0.05 mol % to 1.0 mol %, then decreases with increasing the concentration from 1.0 mol % to about 5.0 mol %, finally becomes nearly zero above 15 mol % (Fig. 7). Unlike the 490, 558, 651, and 736 nm emissions, the quenching concentration is very low (about 1 mol %) in the case of 602 nm emission. Here, the quenching concentration means the concentration from which the emission intensity begins to decrease when Pr^{3+} concentration is increased.

The intensities of the various emissions at 12 K are plotted against the Pr^{3+} concentration in Fig. 8. The 602 nm emission is observed to have a quenching concentration of about 10 mol %. Unlike the 602 nm emission, the 621 nm emission never disappears at high concentrations above 10 mol % (Figs. 8 and 9).

In summary, we have observed three different kinds of concentration dependences for the emissions. The first type is emission with high quenching concentration of about 10 mol % and residual intensity at high concentrations (called Type A, hereafter), the second type is emission with very low quenching concentration of about 1 mol % and residual intensity at high concentrations (Type B-1), and the third type is emission with low quenching concentration of about 1

mol % and zero intensity at high concentrations (Type B-2). The 490, 558, 651, 690, and 736 nm emissions associated with the 3P_0 state belong to Type A, the 621 nm 3P_0 emission belongs to Type B-1, and the 602-608 and 824-830 nm 1D_2 emissions belong to Type B-2 (**Table 1**). Here we have a question “Why do the 490, 558, 651, 690, and 736 nm 3P_0 emissions show not Type B-1 of the 621 nm 3P_0 emission but Type A?”.

According to a theory for the resonant energy transfer due to dipole-dipole interaction between the neighboring rare-earth ions, the emission intensity increases gradually with the increasing concentration, has the maximum, and then gradually decreases, where the quenching concentration depends on rare-earth and host materials.^{5,7,24-26} This concentration dependence is similar to Type A. The quenching starts at much lower concentration (less than 1 mol %) for CR-involved emissions than for CR-free emissions.^{1,3,7,8} Therefore the CR-free 490, 558, 651, 690, and 736 nm 3P_0 emissions of Type A are suggested to arise from the resonant energy transfer, i.e., the energy migration over the Pr^{3+} ions to quenching sites. As a result we understand the reason why the 621 nm 3P_0 emission shows the Type B-1 with quenching at low concentration. The main reason is that unlike the other 3P_0 emission, the 621 nm emission has a CR-involved emission.

3.3.2 The mechanisms of Types B-1 and B-2

We consider the reason why two different Types B-1 and B-2 appear although both tend to quench at almost the same 1 mol %. Three kinds of CRs of ($^3P_0 \rightarrow ^3H_6$):($^3H_4 \rightarrow ^1D_2$), ($^1D_2 \rightarrow ^1G_4$):($^3H_4 \rightarrow ^3F_4$), and ($^1D_2 \rightarrow ^3F_4$):($^3H_4 \rightarrow ^1G_4$) are

conceivable from the Pr^{3+} energy level diagram as shown in **Fig. 4**, where CR of (${}^3\text{P}_0 \rightarrow {}^3\text{H}_6$):(${}^3\text{H}_4 \rightarrow {}^1\text{D}_2$) means that when a Pr^{3+} ion in the ${}^3\text{P}_0$ excited state is relaxed into the lower ${}^3\text{H}_6$ state, a part of its energy is transferred to excite its neighboring Pr^{3+} ion in the ${}^3\text{H}_4$ state into the ${}^1\text{D}_2$ state. Since the energy distance of ${}^1\text{D}_2$ - ${}^1\text{G}_4$ is almost the same 6800 cm^{-1} as the distance of ${}^3\text{H}_4$ - ${}^3\text{F}_4$, and the energy distance of ${}^1\text{D}_2$ - ${}^3\text{F}_4$ is almost the same 9900 cm^{-1} as the distance of ${}^3\text{H}_4$ - ${}^1\text{G}_4$, these CRs are possible.

The ${}^1\text{D}_2 \rightarrow {}^1\text{G}_4$ transition gives emissions at 1486 and 1524 nm, while the ${}^1\text{D}_2 \rightarrow {}^3\text{F}_4$ transition gives an intense emission at 1053 nm (**Fig. 10**). The concentration dependence of the 1053 nm emission (inset of **Fig. 10**) is the same as that of the 1486 and 1524 nm emissions, which belong to the same Type B-2. This is understood as follows. The ${}^1\text{D}_2$ state population is reduced with increasing Pr^{3+} concentration by these two CRs of (${}^1\text{D}_2 \rightarrow {}^1\text{G}_4$):(${}^3\text{H}_4 \rightarrow {}^3\text{F}_4$) and (${}^1\text{D}_2 \rightarrow {}^3\text{F}_4$):(${}^3\text{H}_4 \rightarrow {}^1\text{G}_4$), resulting in the same concentration quenching for all the ${}^1\text{D}_2$ emissions which arise from the ${}^1\text{D}_2$ state. This leads to low quenching concentration for all the ${}^1\text{D}_2$ emissions including the 602 nm emission although the 602 nm emission itself does not have the CR process directly.

Figure 11 shows the decay patterns of 602 nm ${}^1\text{D}_2$ emission for various Pr^{3+} concentrations at room temperature. The decay curve is nearly single exponential at low concentrations, while it becomes non-exponential with increasing concentration. The average lifetime is 47, 38, 35, 18, and 5 μs at 0.05, 0.5, 1.0, 3.0, and 15.0 mol %, respectively. The lifetime decreases nearly exponentially with increasing concentration (inset of **Fig. 11**). These results are consistent with the previous results

for CR-involved emissions obtained from various Pr^{3+} -doped materials,^{2,3,14,27} especially consistent with the experimental results and analysis by Collins et al.² They have analyzed the experimental decay curves of the $^1\text{D}_2$ emission from Pr-doped YPO_4 using the following equation with a zero diffusion constant.

$$I(t) = I_0 \exp[-(t/\tau) - (C/C_0)\Gamma(1/2) (t/\tau)^{1/2}] \quad (1)$$

where τ is the donor lifetime, Γ is the gamma function, C is the concentration of acceptors, and C_0 is the parameter related with critical concentration of acceptors.²

Fig. 11 also shows a comparison of the observed decay curves, which were obtained for the 602 nm $^1\text{D}_2$ emission in BGM, with the calculated curves, which were made using the above equation. Like the case of Collins et al.², a good fitting to the experimental results is obtained with $C_0 = 1.1, 42.4, 86.9,$ and 2331.6 mol % for the Pr^{3+} concentrations of 0.05, 1.0, 3.0, and 15.0 mol %, respectively, although a small deviation is observed at $t > 40$ μs in case of sample with 15.0 mol %. This indicates that (1) the CR rate increases with increasing concentration, and (2) the $^1\text{D}_2$ population is influenced by the CR and not by the energy migration via diffusion process.

The CR also occurs for the $^3\text{P}_0$ state, i.e., CR of $(^3\text{P}_0 \rightarrow ^3\text{H}_6):(^3\text{H}_4 \rightarrow ^1\text{D}_2)$. Therefore, just as the case of the 1053 nm emission, the complete quenching is also expected for the 621 nm $^3\text{P}_0$ emission. The 621 nm emission, however, never disappears even at high concentration of 25 mol % (**Fig. 8**). This unusual concentration quenching is understood as follows.

The energy distance of $^3\text{P}_0$ - $^3\text{H}_6$ is 16000 cm^{-1} , while the energy distance of

${}^3\text{H}_4\text{-}{}^1\text{D}_2$ is 16700 cm^{-1} . There is an energy mismatch in the cross-relaxation of $({}^3\text{P}_0\rightarrow{}^3\text{H}_6):({}^3\text{H}_4\rightarrow{}^1\text{D}_2)$, although that mismatch is small (700 cm^{-1}). This non-resonant (or quasi) CR is allowed by the phonon-assisted transition.^{10,28} The BGM has phonons with energy of about 700 cm^{-1} (**Fig. 2**). This phonon energy is expected to compensate the energy mismatch of 700 cm^{-1} and allow the transition of ${}^3\text{H}_4\rightarrow{}^1\text{D}_2$ by the energy transfer from the transition of ${}^3\text{P}_0\rightarrow{}^3\text{H}_6$. The phonon-assisted thermal excitation is suggested to work effectively at high temperature, but not work effectively at low temperature.¹⁰ Therefore we suggest that the inefficient CR of $({}^3\text{P}_0\rightarrow{}^3\text{H}_6):({}^3\text{H}_4\rightarrow{}^1\text{D}_2)$ at 12 K leads to incomplete ${}^3\text{P}_0$ depopulation even at high concentrations, resulting in the residual intensity for the 621 nm emission at high concentrations. In this way we understand the different concentration dependences between the 621 nm ${}^3\text{P}_0$ emission of Type B-1 and ${}^1\text{D}_2$ emissions of Type B-2.

4. Conclusion

Three types of concentration dependences are observed for the Pr^{3+} emissions. The first type (Type A) has the maximum PL intensity at about 10 mol % with non-zero intensity at high concentrations, which is observed for the ${}^3\text{P}_0$ emissions except emission at 621 nm, while the second and third types (Types B-1 and B-2) have the maximum at about 1 mol % with a finite residual intensity and nearly zero intensity at high concentrations, which are observed for the 621 nm emission and all the ${}^1\text{D}_2$ emissions, respectively. It is suggested that the energy migration mechanism is responsible for the first type, while the resonant cross-relaxation for the second type

and the non-resonant cross-relaxation for the third type. It is found that (1) the resonant cross-relaxation gives rise to the complete 1D_2 depopulation at high concentrations, leading to the nearly complete quenching even for the 1D_2 emissions, which have no cross-relaxation process directly, and (2) the non-resonant cross-relaxation gives rise to incomplete 1D_2 depopulation at high concentrations, leading to residual emission intensity at high concentrations. The PL decay pattern of the 615 nm 1D_2 emission is observed to change from single exponential to non-exponential with increasing the Pr^{3+} concentration, this is in consistent with the CR characteristics.

Acknowledgments

One of the authors, TT, thanks the Japan Society for Promotion of Science for financial support by the Grant-in-Aid for the Scientific Research (Project No. 22560013). He also thanks Dr. Y. Nakata of Horiba, Ltd., Kyoto, Japan for helping the luminescence decay measurement. This work was also supported by A Project Funded by the Priority Academic Program Development of Jiangsu Higher Education Institutions (PAPD).

References

- [1] H. Chen, R. Lian, M. Yin, L. Lou, W. Zhang, S. Xia and J. C. Krupa, *J. Phys.: Condens. Matter*, 2001, **13**, 1151.
- [2] J. Collins, M. Geen, M. Bettinelli and B. Di Bartolo, *J. Limin.*, 2012, **132**, 2626.
- [3] M. Malinowski, M. Kaczkan, S. Turczynski and D. Pawlak, *Opt. Mater.*, 2011, **33**, 1004.
- [4] R. Naccache, F. Vetrone, A. Speghini, M. Bettinelli and J. A. Capobianco, *J. Phys. Chem. C*, 2008, **112**, 7750.
- [5] S. Dai, C. Yu, G. Zhou, J. Zhang, G. Wang and L. Hu, *J. Lumin.*, 2006, **117**, 39.
- [6] N. Jaba, H. BenMansour, A. Kanoun, A. Brenier and B. Champagnon, *J. Lumen.*, 2009, **129**, 270.
- [7] Z. Y. Mao, Y. C. Zhu, Y. Zeng, L. Gan and Y. Wang, *J. Lumen.*, 2013, in press.
- [8] A. D. Sontakke and K. Annapurna, *Mater. Chem. Phys.*, 2013, **137**, 916.
- [9] T. Luxbacher, H. P. Fritzer and C. D. Flint, *J. Lumin.*, 1997, **71**, 177.
- [10] M. Kaczkan, Z. Boruc, B. Fetlinski, S. Turczynski and M. Malinowski, *Appl. Phys. B*, 2013, published online.
- [11] M. Voda, R. Balda, M. Al-Saleh, I. Saez de Ocariz, M. Cano and J. Fernandez, *J. Alloys Comp.*, 2001, **323-324**, 250.
- [12] M. Voda, R. Balda, I. Saez de Ocariz, L. M. Lacha, M. A. Illarramendi and J. Fernandez, *J. Alloys Comp.*, 1998, **275-277**, 214.
- [13] R. C. Naik, N. P. Karanjikar and M. A. N. Razvi, *J. Lumin.*, 1992, **54**, 139.
- [14] H. Zhu, Y. Chen, Y. Lin, X. Gong, Z. Luo and Y. Huang, *J. Opt. Soc. Am. B*, 2007, **24**, 265.
- [15] Y. Pan, Y. J. Chen and J. H. Huang, *Opt. Mater.*, 2012, **34**, 1143.

- [16] D. Zhao, Z. Lin, L. Zhang and G. Wang, *J. Phys. D: Appl. Phys.*, 2007, **40**, 101.
- [17] M. M. Haque and D. -K. Kim, *Mater. Lett.*, 2009, **63**, 793.
- [18] A. A. Kaminskii, H. Nishioka, K. Ueda, W. Odajimu, M. Tateno, Y. Sasaki and S. N. Bagayev, *Laser Phys.*, 1996, **6**, 817.
- [19] W. Zhao, W. Zhou, R. Zhuang, G. Wang, J. Du, H. Yu, Z. Lv, F. Wang and Y. Chen, *Mater. Research Innovations*, 2012, **16**, 237.
- [20] G. S. Ofelt, *J. Chem. Phys.*, 1962, **37**, 511.
- [21] B. Chen, Y. Luo, H. Liang and X. Liu, *Spectrochimica Acta A*, 2008, **70**, 1203.
- [22] H. Wen, G. Jia, C. K. Duan and P. A. Tanner, *Phys. Chem. Chem. Phys.*, 2010, **12**, 9933.
- [23] G. H. Dieke and H. M. Crosswhite, *Appl. Optics*, 1963, **2**, 675.
- [24] T. Kushida, *J. Phys. Soc. Jpn.*, 1973, **34**, 1327.
- [25] S. Tanabe, *Rare Earths*, 1993, **23**, 67.
- [26] T. Kushida, *J. Phys. Soc. Jpn.*, 1973, **34**, 1318.
- [27] Z. G. Mazurak, J. P. M. van Vliet and G. Blasse, *J. Solid State Chem.*, 1987, **68**, 227.
- [28] J. Su, F. Song, H. Tao, L. Han, F. Zhou, J. Tian and H. Chen, *J. Phys. D: Appl. Phys.*, 2006, **39**, 2094.

Table 1 Concentration dependences of the intensities from the Pr^{3+} emissions in BGM, with the responsible mechanisms

Type	$^3\text{P}_0$ emission	$^1\text{D}_2$ emission	Mechanism
A	490, 558, 651, 690, 736 nm emission		Energy migration
B-1	621 nm emission		Non-resonant CR
B-2		602, 608, 615, 830, 1053, 1486, 1524 nm emission	Resonant CR

Type A: quenching at high concentration and residual intensity at high concentrations

Type B-1: quenching at low concentration and residual intensity at high concentrations

Type B-2: quenching at low concentration and zero intensity at high concentrations

Figures and Captions

Fig. 1 XRD patterns of the samples PrN (N=1, 3, 5, 6, 8, and 10) with different Pr³⁺ concentrations (0.05, 1.0, 5.0, 7.0, 15, and 25 mol %, respectively) in BaGd₂(MoO₄)₄ at room temperature. Except for a few impurities (*), all peaks could be indexed according to the PDF#2 No: 36-0192.

Fig. 2 Unpolarized spontaneous Raman spectra of Pr1, Pr6, Pr9, and Pr10 with 0.05, 7.0, 20, and 25 mol % Pr³⁺ concentrations, respectively, at room temperature.

Fig. 3 PL spectra of Pr2 with 0.5 mol % Pr³⁺ concentration, which were excited at 450 nm at room temperature and 12 K. The spectra were measured with a resolution of 1 nm.

Fig. 4 Schematic energy level diagram of Pr³⁺ and the assignments for the observed emissions at 12 K. Oblique line indicates the cross-relaxation.

Fig. 5 PLE spectra of Pr2 with 0.5 mol % Pr³⁺ concentration for 690 and 736 nm emissions at 12 K.

Fig. 6 PL spectra of Pr³⁺-doped BGM with various Pr³⁺ concentrations from 0.05 mol % to 25 mol %, which were excited at 450 nm at room temperature.

Fig. 7 The intensities of the emissions at 602 and 651 nm plotted against Pr³⁺ concentration. The emissions were obtained under excitation at 450 nm at room temperature. The 602 nm emission intensity is enlarged by two times.

Fig. 8 The intensities of the emissions at 558, 602, 621, and 651 nm plotted against Pr³⁺ concentration. The emissions were obtained under excitation at 450 nm at 12 K. The 602 and 621 nm emission intensities are enlarged by two times.

Fig. 9 PL spectra of Pr1, Pr2, Pr4, and Pr10 with 0.05, 0.5, 3.0, and 25.0 mol % Pr³⁺ concentrations, respectively, which were excited at 450 nm at 12 K. The spectra are normalized at the peak intensity of the 651 nm emission line.

Fig. 10 Infrared PL spectrum of Pr2 with 0.5 mol % Pr³⁺ concentration, which was excited at 593 nm at 12 K. Inset is the concentration dependence of the 1053 nm emission intensity.

Fig. 11 Decay curves of the 602 nm Pr³⁺ emission in BGMs with various Pr³⁺ concentrations. Excitation was made at room temperature by pulsed 450 nm light with 1 ns pulse width. The dots show the calculated decay which fits to the observed decay curve. Inset plots the average lifetime against the Pr³⁺ concentration.

Fig. 1 XRD patterns of the samples PrN (N=1, 3, 5, 6, 8, and 10) with different Pr³⁺ concentrations (0.05, 1.0, 5.0, 7.0, 15, and 25 mol %, respectively) in BaGd₂(MoO₄)₄ at room temperature. Except for a few impurities (*), all peaks could be indexed according to the PDF#2 No: 36-0192.

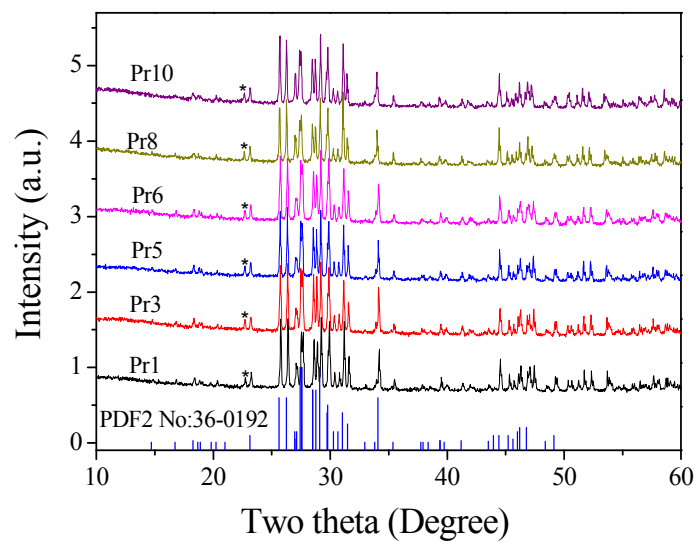


Fig. 2 Unpolarized spontaneous Raman spectra of Pr1, Pr6, Pr9, and Pr10 with 0.05, 7.0, 20, and 25 mol % Pr³⁺ concentrations, respectively, at room temperature.

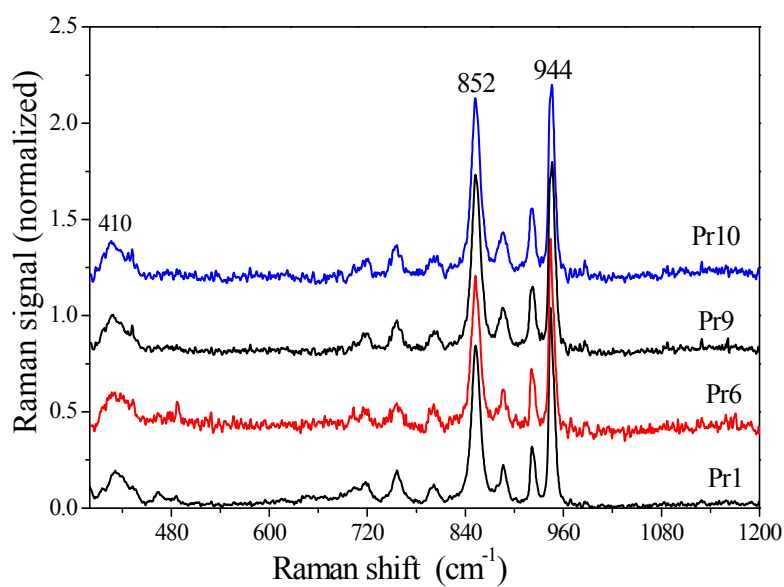


Fig. 3 PL spectra of Pr₂ with 0.5 mol % Pr³⁺ concentration, which were excited at 450 nm at room temperature and 12 K. The spectra were measured with a resolution of 1 nm. The number like 490 means the emission peak wavelength 490 nm.

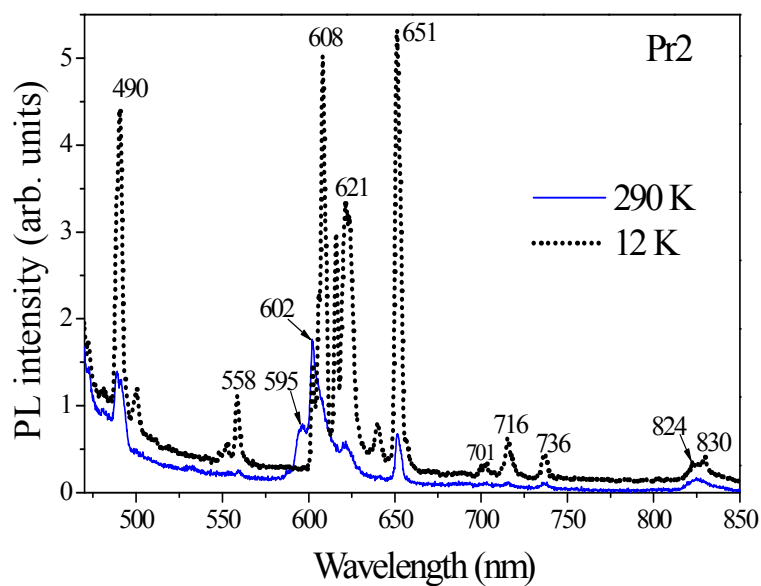


Fig. 4 Schematic energy level diagram of Pr^{3+} and the assignments for the observed emissions at 12 K. Oblique line indicates the cross-relaxation. The number like 621 means the emission peak wavelength 621 nm.

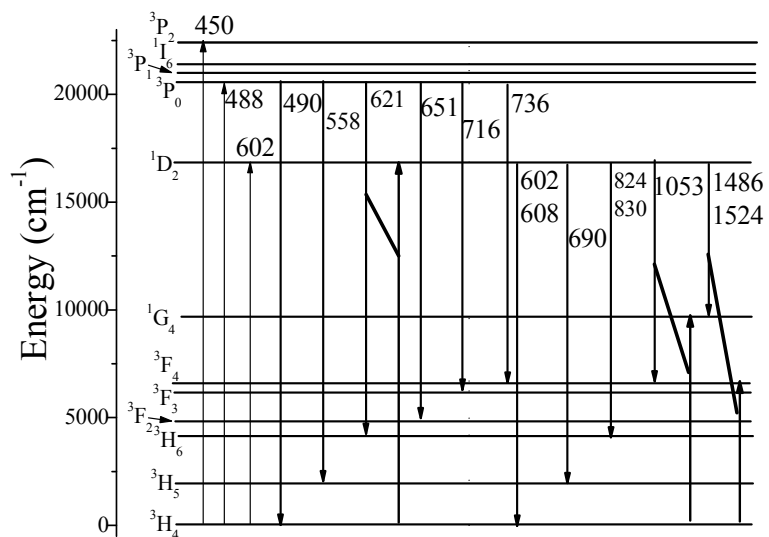


Fig. 5 PLE spectra of Pr₂ with 0.5 mol % Pr³⁺ concentration for 690 and 736 nm emissions at 12 K.

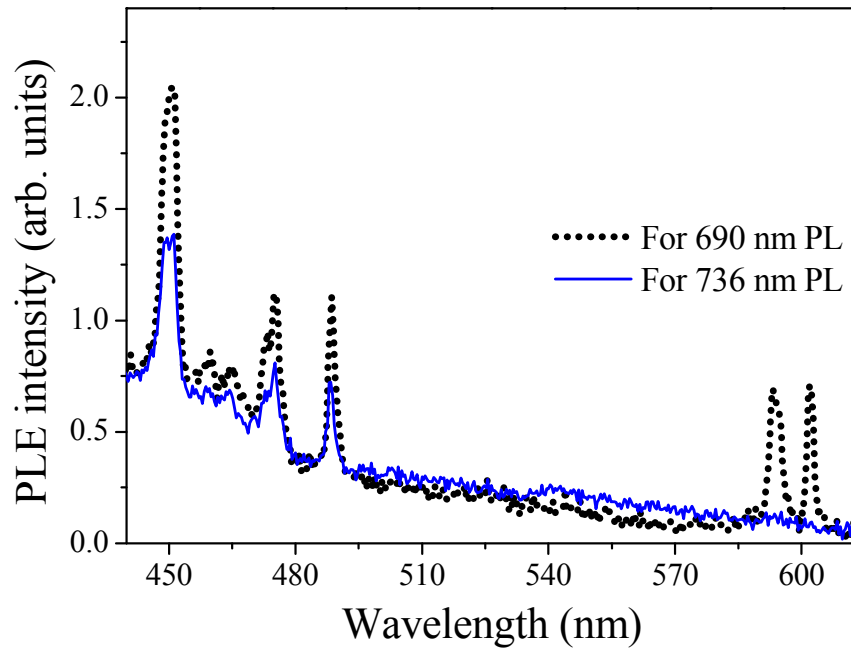


Fig. 6 PL spectra of Pr³⁺-doped BGM with various Pr³⁺ concentrations from 0.05 mol % to 25 mol %, which were excited at 450 nm at room temperature.

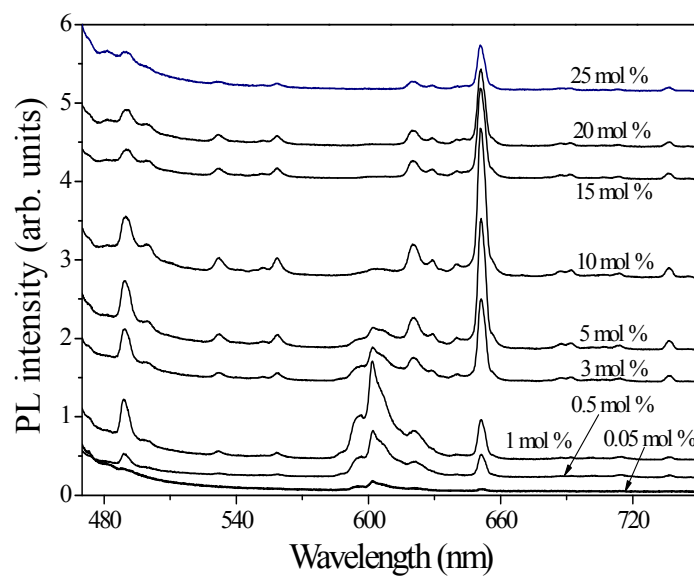


Fig. 7 The intensities of the emissions at 602 and 651 nm plotted against Pr^{3+} concentration. The emissions were obtained under excitation at 450 nm at room temperature. The 602 nm emission intensity is enlarged by two times.

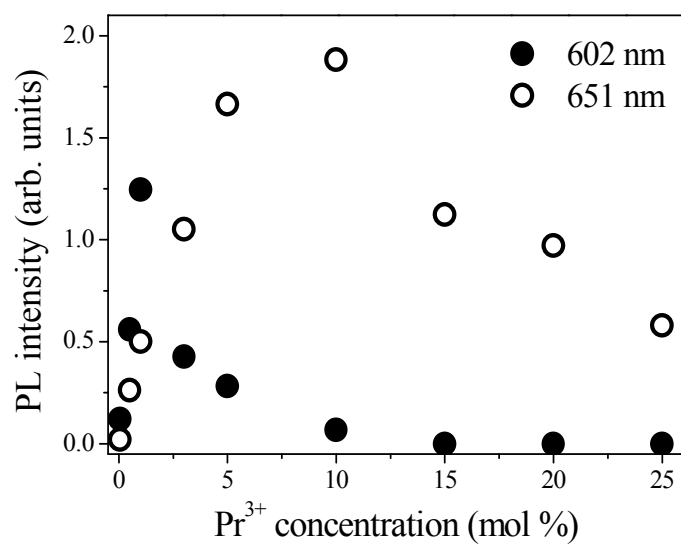


Fig. 8 The intensities of the emissions at 558, 602, 621, and 651 nm plotted against Pr^{3+} concentration. The emissions were obtained under excitation at 450 nm at 12 K. The 602 and 621 nm emission intensities are enlarged by two times.

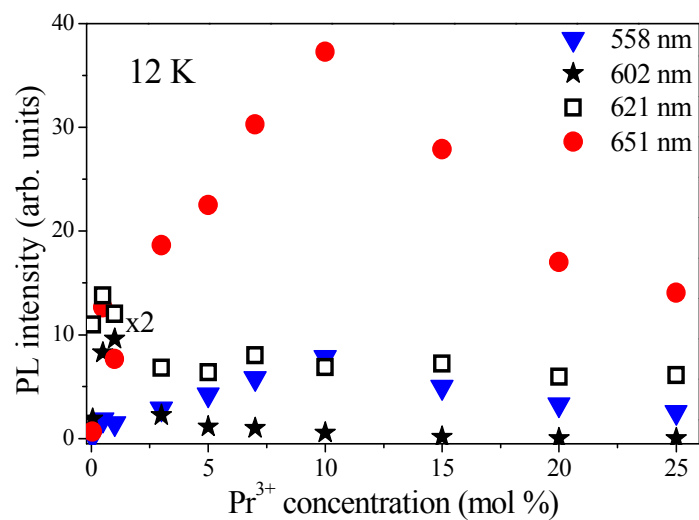


Fig. 9 PL spectra of Pr1, Pr2, Pr4, and Pr10 with 0.05, 0.5, 3.0, and 25.0 mol % Pr³⁺ concentrations, respectively, which were excited at 450 nm at 12 K. The spectra are normalized at the peak intensity of the 651 nm emission line.

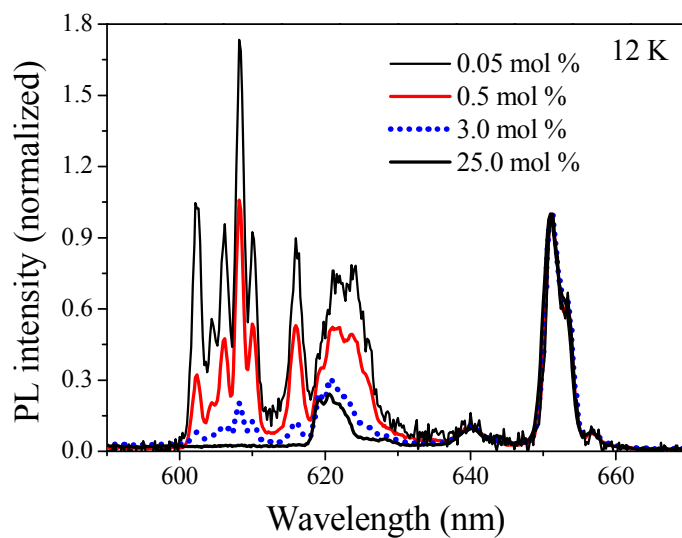


Fig. 10 Infrared PL spectrum of Pr₂ with 0.5 mol % Pr³⁺ concentration, which was excited at 593 nm at 12 K. Inset is the concentration dependence of the 1053 nm emission intensity.

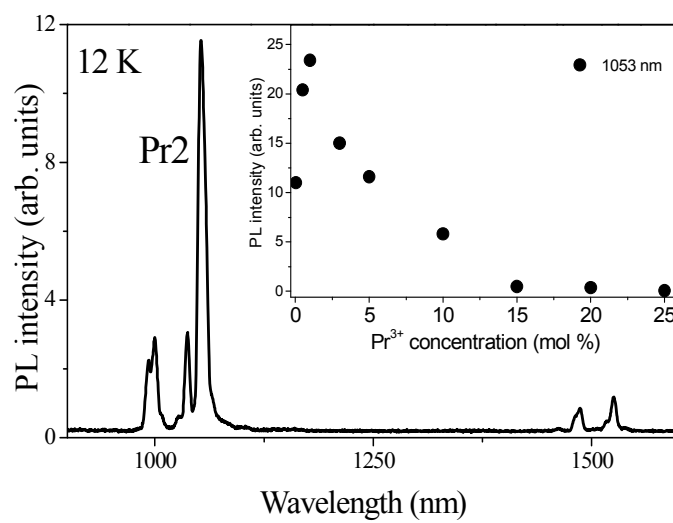


Fig. 11 Decay curves of the 602 nm Pr^{3+} emission in BGMs with various Pr^{3+} concentrations. Excitation was made at room temperature by pulsed 450 nm light with 1 ns pulse width. The dots show the calculated decay which fits to the observed decay curves. Inset plots the average lifetime against the Pr^{3+} concentration.

